J Mater Sci: Mater Med (2011) 22:2131–2138
DOI 10.1007/s10856-011-4393-5

Long-term in vivo response to citric acid-based nanocomposites for orthopaedic tissue engineering

Eun Ji Chung · Pradeep Kodali · William Laskin · Jason L. Koh · Guillermo A. Ameer

Received: 16 December 2010 / Accepted: 9 July 2011 / Published online: 24 July 2011

Abstract The disadvantages of current bone grafts have triggered the development of a variety of natural and synthetic bone substitutes. Previously, we have described the fabrication, characterization, and short-term tissue response of poly(1,8-octanediol-co-citrate) (POC) with 60 weight % hydroxyapatite nanocrystals (POC-HA) at 6 weeks. In order to better understand the clinical potential, longer term effects, and the biodegradation, biocompatibility, and bone regenerative properties of these novel nanocomposites, POC-HA, POC, and poly-L-lactide (PLL) were implanted in osteochondral defects in a rabbit model and assessed at 26 weeks. Explants were stained with Masson Goldner Trichrome and the fibrous capsule and tissue ingrowth measured. In addition, the bone-implant and bone-cartilage response of POC-HA, POC, and PLL were assessed through histomorphometry and histological scoring. Upon histological evaluation, both POC-HA and POC implants were biocompatible, but PLL implants were surrounded by a layer of leukocytes at 26 weeks. In addition, due to the degradation properties of POC-HA, tissue grew into the implant and had the highest area of tissue ingrowth although not statistically significant. Histomorphometric analyses supported a similar osteoid, osteoblast, and trabecular bone surface area among all implants although the fibrous capsule thickness was the largest for POC. Moreover, histological scoring demonstrated comparable scores among all three groups of the articular cartilage and subchondral bone. This study provides the long-term bone and cartilage response of novel, citric acid-based nanocomposites and their equivalence to FDA-approved biomaterials. Furthermore, we provide new insights and further discussion of these nanocomposites for orthopaedic applications.

Electronic supplementary material The online version of this article (doi:10.1007/s10856-011-4393-5) contains supplementary material, which is available to authorized users.

E. J. Chung and P. Kodali contributed equally to this work.

E. J. Chung
Department of Biomedical Engineering, Northwestern University, 2145 Sheridan Rd, Room E310, Evanston, IL 60208, USA

P. Kodali
Department of Orthopaedic Surgery, University of Texas Medical School at Houston, 6400 Fannin, Suite 1700, Houston, TX 77030, USA

W. Laskin
Department of Pathology, Feinberg School of Medicine, Northwestern University, 710 N. Fairbanks Court, Chicago, IL 60611, USA

J. L. Koh
Department of Orthopaedic Surgery, University of Chicago, NorthShore University Health System, 1000 Central St, Evanston, IL 60201, USA

G. A. Ameer (✉)
Department of Biomedical Engineering, Department of Surgery, The Institute for BioNanotechnology in Medicine, Chemistry for Life Processes Institute, Northwestern University, 2145 Sheridan Rd, Room E310, Evanston, IL 60208, USA
e-mail: g-ameer@northwestern.edu

1 Introduction

The emergence of synthetic bone graft substitutes for bone defects is in response to the disadvantages inherent to autografts and allografts, which include donor site morbidity, supply limitations, and disease transmission [1]. While earlier biomaterials aimed to restore basic functions by simply filling in the voids, increasingly, biomaterials are

designed to provide both mechanical support as well as biological repair. In addition, these materials can target biological responses such as osteoconductivity so that osteoprogenitor cells can adhere and differentiate to form new bone [2–5].

Composites consisting of biodegradable polymers and hydroxyapatite (HA) nanocrystals have been developed as bone replacements, incorporating the biocompatible and controllable degradation properties of polymers with the osteoconductive, bioactive, and bone-bonding properties of HA [3, 6]. In addition, the inherent brittleness and difficulty for processing HA and the acidic degradation products of many polymers are bypassed through their combination [7–9]. The mineral content also provides stiffness to the resulting composite, while the polymer provides degradability to allow for host tissue replacement over time [10, 11]. Moreover, bone is a natural nanocomposite itself with 60–70% by weight HA nanocrystals embedded within primarily a collagen-containing organic phase [10, 12, 13]. Therefore, biodegradable nanocomposites can further mimic the structure, components, and properties of bone.

Previously, we have described the fabrication, mechanical properties, and 6-week bone response to biodegradable, citric acid-based elastomers containing up to 60% by weight of either microparticle or nanoparticle HA [9, 14]. Poly(1,8-octanediol-co-citrate) (POC) was found to be an adequate macrophase polymeric binder for both particle types [9]. Elastomers, such as POC, as the matrix phase are advantageous over thermoplastics because these elastomers have a low stiffness which is favorable for high % of particle reinforcement without the harmful effects of stress-shielding [15]. The mechanical properties of the nanocomposites, however, were closer to those of human trabecular bone which is attributable to an increase in stiffness with the decrease in particle size, in addition to the physical interlock that is provided between the spindle-shaped, nanometer-sized HA and the polymeric matrix [9, 13, 16, 17]. In vivo, all composites displayed good biocompatibility and the fibrous capsule thicknesses were minimal, but histomorphometric analyses suggested a higher rate of bone regeneration for POC nanocomposites with 60% HA (POC-HA) at 6 weeks [9]. Although those results are promising, a long-term in vivo assessment of these materials as bone replacements is needed to understand the biodegradation behavior and bone remodeling potential of the implant [18–20]. Herein, we evaluate the 26-week biocompatibility and bone-implant and cartilage-implant interfacial response to POC-HA in an osteochondral defect in a rabbit model. These longer-term in vivo assessments will confirm both the safety of these novel biomaterials and their potential utility in clinical applications.

2 Methods and materials

2.1 Composite fabrication

Synthesis of the POC prepolymer and the fabrication method of POC–HA nanocomposites have been reported elsewhere [9, 21]. Briefly, POC prepolymer (MW: 1088) was synthesized via a condensation reaction of 1,8-octanediol and citric acid (1 to 1 mol ratio, Sigma Aldrich, St Louis, MO, USA) and then mixed with 60% by weight HA nanoparticles (medical grade, 100 nm, Berkeley Advanced Biomaterials, Berkeley, CA, USA) to obtain POC-HA composites. The resulting clay-like mass was post-polymerized at 80°C for 3 days and 120°C for 1 day under vacuum.

2.2 Implantation

Solid, cylindrical POC–HA nanocomposites, POC, and poly-L-lactide (PLL) plugs with a diameter of 2.7 mm and a length of 4.0 mm were shaped using a mosaicplasty harvester (Smith and Nephew, Memphis, TN, USA). PLL plugs were chosen as a control because of its widespread use as fixation devices and were machined from biodegradable, interference screws (MW: 350 ± 10 kDa, Arthrex, Naples, FL, USA). Samples were sterilized using an AN74j/Anprolene ethylene oxide sterilization system that performed a 24 h degassing step under vacuum after gas exposure (Anderson Sterilization, Inc., Haw River, NC, USA).

Three experimental groups consisting of three skeletally-mature, male New Zealand rabbits (weighing between 2.3 and 2.7 kg) were investigated (Covance, Kalamazoo, MI, USA): POC-HA, POC, and PLL. The surgical protocol follows National Institute of Health guidelines for the care and use of laboratory animals and was approved by Northwestern University's Animal Care and Use Committee. Briefly, anesthesia was induced with an intramuscular injection of ketamine (40 mg/kg) and xylazine (5–7 mg/kg) and maintained with isoflurane (1–2% inhalation). After shaving and sterilely prepping both lower extremities, a 4 cm medial parapatellar arthrotomy was created in each knee, exposing the medial femoral condyle. Using a mosaicplasty harvester, a bone defect with dimensions 2.7 mm (diameter) × 4.0 mm (depth) was created in medial femoral condyles and filled with the appropriate implant. Each group consisted of three knees from the same side. All rabbits were allowed to ambulate freely postoperatively.

2.3 Characterization of the tissue–implant interface

At 26 weeks, the distal femur was harvested and gross examination was documented using a digital camera

(Fig. 1). All explants were immediately fixed in 10% neutral-buffered formalin, dehydrated in graded series of ethanol, and embedded using the JB-4 plus embedding kit (Polysciences, Warrington, PA, USA). All specimens were sectioned at 5–10 μm longitudinal thickness for histological assessment using a HM 355 S Rotary Microtome (Richard-Allan Scientific, Kalamazoo, MI, USA) and stained with Masson Goldner Trichrome staining.

Sections were assessed via standard light microscopy (Nikon Eclipse TE2000-U, Melville, NY, USA). The total area and range of depth of tissue ingrowth were measured all around each sample. Three sections were used per sample and measurements from a total of nine sections were averaged for each group. For histomorphometric analyses, the following variables were quantified as previously recorded: (1) ratio of active osteoid surface area to total trabecular bone surface area; (2) ratio of total osteoid surface area to total trabecular bone surface area; and (3) the ratio of trabecular bone surface area to total tissue area [9]. All tissue–implant interfaces were analyzed at 200× magnification with 20 random fields of view of $200 \times 200\ \mu m^2$ starting from the edge of the implant. Three sections per sample were analyzed for a total of nine sections per group.

At 26 weeks, the fibrous capsule widths were also measured. Ten random fibrous capsule widths were taken from around the implant and three sections were used for each sample. Therefore, a total of 90 measurements were averaged for each group. All measurements in this study were performed using Image-Pro Plus v. 5.0 (Media Cybernetics, Silver Spring, MD, USA).

In addition to bone-implant interfacial analysis, the tissue regenerated above the implant was evaluated with histology scoring adopted from Niederauer et al. [22]. The histological scoring system used for evaluating osteochondral defects takes into account the predominant type of tissue formed, and scores structural integrity, thickness, and cellularity of the regenerated cartilage, as well as the degree of subchondral bone regeneration and inflammatory response at the subchondral bone interface (Table 1). All histology scoring was performed blindly by a pathologist.

2.4 Statistical analysis

Analysis of variance (ANOVA) with Newman-Keuls multiple comparison test post-hoc analysis was used to determine significant differences among three or more means. A student's *t*-test was used to compare pairs of means. All analyses were performed using GraphPad Prism 4.0 (La Jolla, CA, USA), and a *P*-value of 0.05 or less was considered to be significant.

A power analysis revealed that three animals would provide 80% power to detect a median difference of 16.5%. This was based on a standard deviation of 5%, which has been previously reported [23, 24].

3 Results

3.1 Gross evaluation and histological assessment

At 26 weeks, all implants were found to be biocompatible upon gross examination. There was no evidence of wound

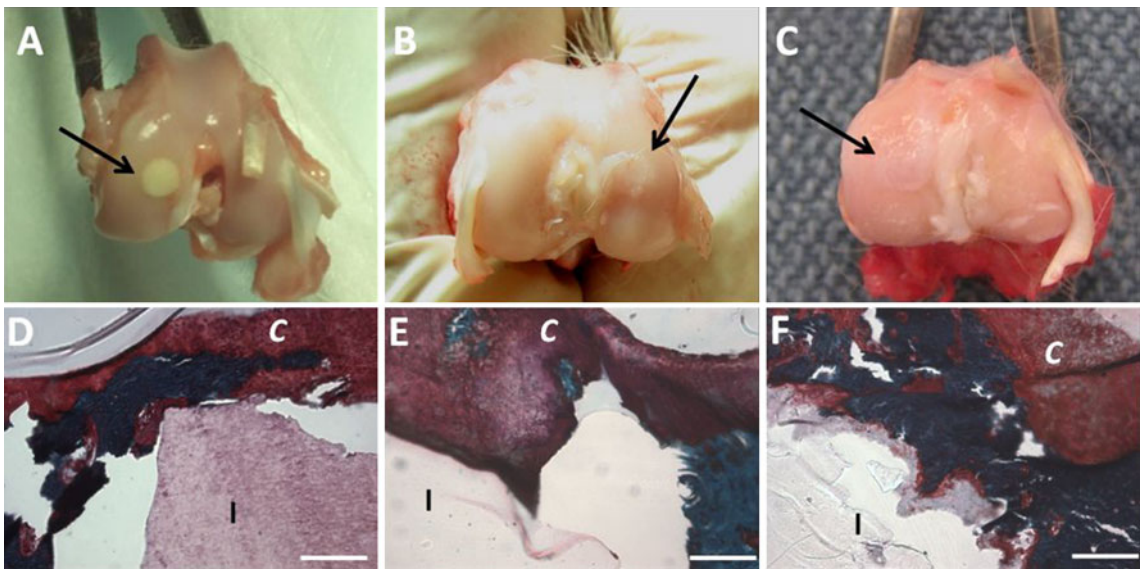

Fig. 1 Gross examination and Masson Goldner Trichrome staining of the osteochondral junction of **a**, **d** POC-HA, **b**, **e** POC, and **c**, **f** PLL implants at 26 weeks; *arrows point* over the implant site covered with a layer of cartilage, *I* implant, *C* cartilage. *SB* 500 μm

Table 1 Histology scoring scale for osteochondral defects [22]

	Characteristic		Score
I.	Nature of predominant Tissue	Hyaline cartilage	4
		Mostly hyaline cartilage	3
		Mixed hyaline and fibrocartilage	2
		Mostly fibrocartilage	1
		Some fibrocartilage, mostly nonchondrocytic cells	0
II.	Structural characteristics		
	A. Surface regularity	Smooth and intact	3
		Superficial horizontal lamination	2
		Fissures	1
		Severe disruption, including fibrillation	0
	B. Structural Integrity, homogeneity	Normal	2
		Slight disruption, including cysts	1
		Severe disintegration, disruptions	0
	C. Thickness	100% of normal adjacent cartilage	2
		50–100% of normal cartilage	1
		0–50% of normal cartilage	0
	D. Bonding to adjacent cartilage	Bonded at both ends of graft	2
		Bonded at one end or partially at both ends	1
		Not bonded	0
III.	Freedom from cellular changes of degeneration		
	A. Hypocellularity	Normal cellularity	2
		Slight hypocellularity	1
		Moderate hypocellularity or hypercellularity	0
	B. Chondrocyte clustering	No clusters	2
		<25% of cells	1
		25–100% of cells	0
IV.	Freedom from degenerative changes in adjacent cartilage		
		Normal cellularity, no clusters, normal staining	3
		Normal cellularity, mild clusters, moderate staining	2
		Mild or moderate hypo/hypercellularity, slight staining	1
		Severe hypocellularity, poor or no staining	0
V.	Subchondral Bone		
	A. Reconstruction of subchondral bone	Normal	3
		Reduced	2
		Minimal	1
		None	0
	B. Inflammatory response in subchondral bone region		
		None/mild	2
		Moderate	1
		Severe	0
		Total Score	25

infection at the implant site, and all rabbits recovered well without any signs of erythema, swelling, or sinus tract formation. After exposing the medial femoral condyle, a continuous, cartilaginous layer covered the surface of the implants (Fig. 1a–c). The surrounding articular cartilage, ipsilateral meniscus, and tibial articular surface did not show any evidence of degeneration and the implant did not show any signs of loosening. Upon histological evaluation, no inflammation or the presence of macrophages or giant cells were observed at the implant-bone or implant-cartilage interface with the exception of the PLL group (Figs. 1d–f, 2). All rabbit knees with PLL implants were

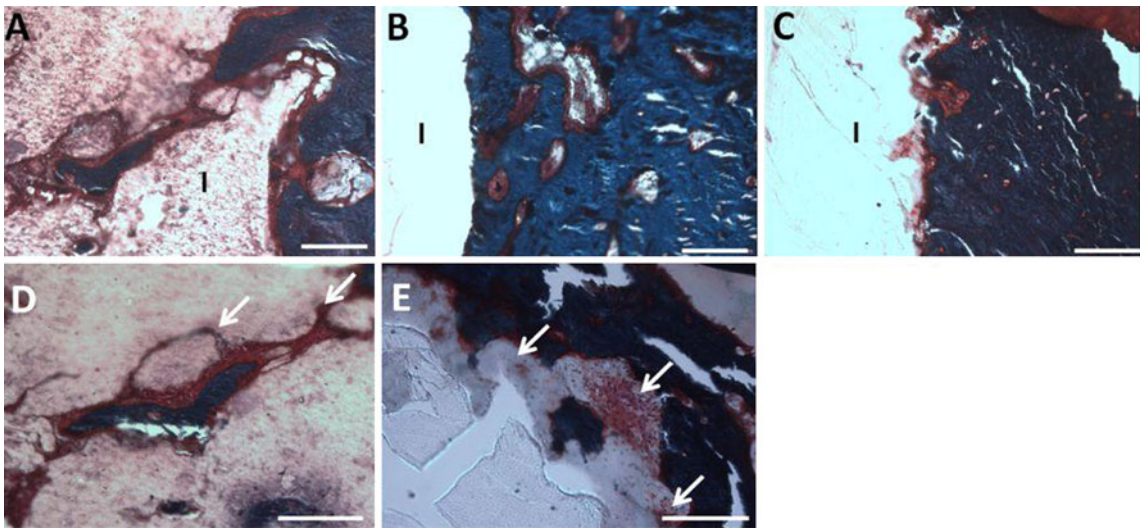

Fig. 2 Representative Masson Goldner Trichrome staining of the bone-implant interface for **a** POC-HA, **b** POC, and **c** PLL at 26 weeks; *I* implant. *SB* 200 μm. High magnification displaying the presence of **d** vascularization (*arrows*) in POC-HA implants and **e** leukocytes (*arrows*) around PLL implants. *SB* 200 μm

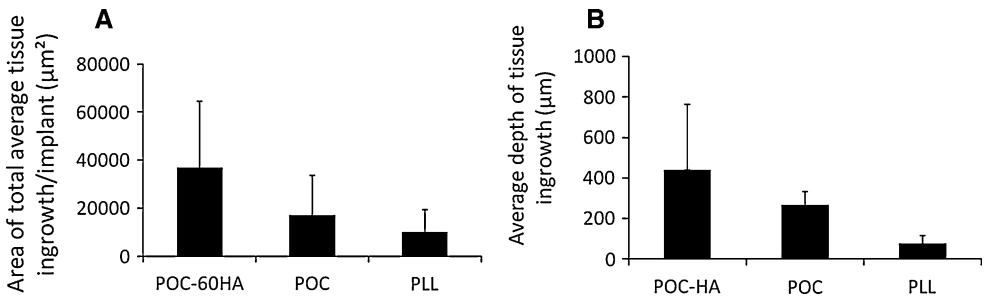

Fig. 3 Average **a** area and **b** depth of tissue ingrowth into the implant at 26 weeks. No significant differences were found for all parameters ($N = 3$ animals, 9 sections/group; ±SD of the mean)

found to have a thin layer of leukocytes around the implant (Fig. 2c, e). Tissue ingrowth was prominent in the POC-HA samples and notably, one POC-HA sample also displayed vascularization within the implant (Fig. 2a, d). The area of tissue ingrowth into the implant and the average depth of tissue ingrowth for all implants at 26 weeks were similar among all samples and were not found to be statistically significant (Fig. 3a, b).

3.2 Histomorphometry and fibrous capsule quantitative analysis of the bone-implant interface

Histomorphometric measurements for osteoid surface area, active osteoblast surface area, and trabecular bone surface area were analyzed for all composites (Fig. 4). No significant differences were found among all implants for all three parameters, although POC-HA samples had a higher average of osteoblast and trabecular bone surface area and PLL samples displayed the highest osteoid surface area; POC samples displayed the lowest value for all three parameters. The fibrous capsule thickness was the largest for POC and the smallest for POC-HA, although this was not found to be significantly different for all three groups (Fig. 5). Moreover, the fibrous capsule for all three groups was discontinuous around each implant. The trend for fibrous capsule thickness was POC>PLL>POC-HA.

3.3 Histology scoring of osteochondral-implant interface

All groups displayed articular cartilage growth and subchondral bone regeneration above the implant. Histology scoring demonstrated comparable scores among all three groups and ranked at the 75–76th percentile of the maximum score (Fig. 6).

4 Discussion

With the growing elderly population and the rise in sports-related injuries, a variety of synthetic implants for

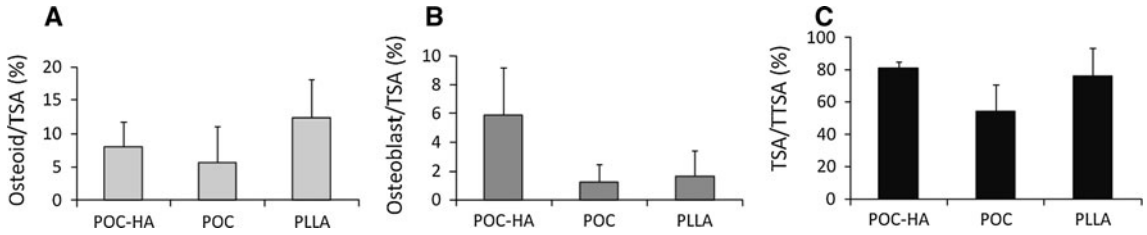

Fig. 4 Histomorphometry analysis of all implants including **a** total osteoid surface area divided by the total trabecular surface area of implants, **b** active osteoblasts surface area divided by the total trabecular surface area of implants, and **c** total trabecular bone surface area divided by the total tissue surface area of implants. No significant differences were found for all parameters ($N = 3$ animals, 9 sections, 180 images/group; ±SD of the mean)

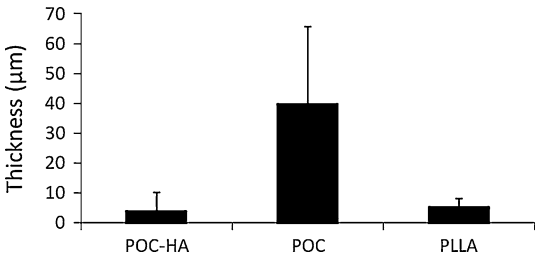

Fig. 5 Average fibrous capsule thicknesses of all implants at 26 weeks. No significant differences were found ($N = 3$ animals, 9 sections, 90 measurements/group; ±SD of the mean)

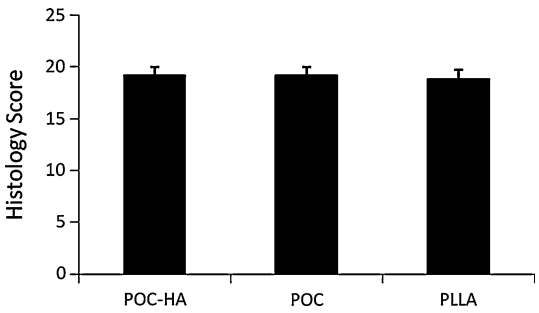

Fig. 6 Histological scoring of the articular cartilage above all implants at 26 weeks (max score = 25). No significant differences were found ($N = 3$ animals, 3 sections; ±SD of the mean)

orthopedic applications have been developed. The vast majority of orthopaedic implants are metallic implants that are far from ideal. The lack of integration, mechanical mismatch, and unwanted tissue reactions make them permanent, stress-shielding implants that weaken the surrounding bone and can lead to significant bone removal through secondary intervention [25–27]. Alternatively, the incorporation of calcium phosphate ceramics such as HA has been combined with biodegradable polymers (i.e. PLL) in order to enhance osteointegration, mechanical strength, and biodegradability [18]. Nonetheless, these materials have slow degradation rates, relatively high costs in comparison to their metallic counterparts, and late aseptic inflammatory reactions [28–31].

Previously, we described the fabrication, material properties, and short-term tissue response to POC-HA nanocomposites in a rabbit osteochondral defect [9]. The favorable mechanical and bone regenerative properties were encouraging, but long-term in vivo studies assessing the biocompatibility, biodegradation behavior, and implant-tissue response of these devices are necessary in order to better assess its full potential for clinical application. Herein we report on the long-term in vivo assessment of these bioceramic-elastomer nanocomposites.

At 26 weeks post-implantation, histology results confirmed that the osteocyte morphology and arrangement surrounding all implants appeared normal and little or no inflammatory response to POC and POC-HA implants was found (Fig. 1, 2). In contrast, leukocytes were in close proximity to the PLL implants for all animals, a phenomenon that was not observed in PLL samples in the previously reported 6-week study. These findings are consistent with many studies that investigated late tissue response to implants [32–36]. The fibrous capsule thickness of POC-HA composites was discontinuous, minimal, and comparable to PLL at both 26 and 6 weeks (Fig. 5) [9]. Although not statistically significant among the groups, POC samples displayed a relatively thick fibrous tissue of 39.5 µm (POC-HA: 4.0 µm, PLL: 5.2 µm). However, when compared to fibrous capsule thicknesses of POC implants from the 6 week study (130.2 µm), the thickness at 26 weeks was significantly reduced [9].

The area of tissue ingrowth was the largest for POC-HA although this value was not statistically significant at 26 weeks (Fig. 3). However, by one year, the tissue ingrowth increased for POC-HA and PLL samples and the area of tissue ingrowth into POC-HA was 288% higher than PLL samples and found to be statistically significant ($P < 0.05$, Supplementary Fig. 1). Tissue ingrowth in POC-HA samples confirms in vivo degradation properties of the nanocomposite and their osteoconductivity (Fig. 2). Although POC-HA implants were not initially porous, the POC component is degradable and a blend between two materials with different degradation characteristics may induce degradation discrepancies at the surface which may

lead to the formation of pores over time [37]. These characteristics contribute to the favorable tissue response of POC-HA nanocomposites, in contrast to other polyester biomaterials susceptible to bulk degradation [38, 39]. Moreover, one POC-HA sample displayed vascularization around and within the implant (Fig. 2D). Although this may be an outlier, many groups have shown that calcium phosphate-based scaffolds can support vascular structures and further studies to examine the angiogenic potential of POC-HA are needed, [40–44].

Histomorphometric analyses did not identify any significant differences among POC-HA, POC, and PLL groups (Fig. 4). Nonetheless, osteoblast and trabecular bone content was the highest for POC-HA emphasizing its bioactivity and bone regenerative properties at 26 weeks, and their equivalence to PLL. Furthermore, an increase in mineralized tissue without the enhancement of osteoid parallels results from Murphy and colleagues in which implants that induced angiogenesis could increase maturation of infiltrating osteoblasts during bone development [42]. POC had the lowest osteoblast, osteoid, and trabecular surface area and these values for all three implant groups did not change significantly when compared to results obtained at 6 weeks [9].

Concurrently, gross evaluation exhibited fully regenerated articular cartilage above the implant at 26 weeks and subchondral bone was healthy (Fig. 1). These findings confirm the potential utility of these implants for complex tissues in which both cartilage and bone, and both soft and hard tissues must be regenerated. In order to assess whether POC-HA would be appropriate as scaffolds for osteochondral repair, histology scoring considering both the subchondral bone and the articular cartilage was conducted in a rabbit model [20]. Histology scores for POC-HA are comparable to both POC and PLL implant groups, significant differences were not observed, and are comparable to other biomaterials designed for osteochondral repair (Fig. 6) [22]. Although the rabbit model is often used for assessing osteochondral repair, the occurrence of spontaneous cartilage regeneration may hinder a perfect correlation for human applications [45]. Nonetheless, these initial studies validate the substantial equivalence of POC-HA to PLL at 26 weeks, a polymer used in FDA-approved fixation devices. By 52 weeks, tissue ingrowth into POC-HA is increased in comparison to PLL, which highlights an additional benefit of these novel biomaterials. Furthermore, the development and application of a biphasic scaffold that consists of POC to support cartilage growth and POC-HA to support subchondral bone growth may also be used in future applications to improve the outcome of osteochondral repairs [46]. Collectively, these results confirm the potential utility of POC-HA for bone substitutes and fixation devices.

5 Conclusion

The 26-week invivo response of biomimetic nanocomposites based on citric acid and HA nanocrystals exhibited integration with and regeneration of bone. Histomorphometric analysis at the bone-implant interface revealed higher trabecular bone and osteoblast surface fractions for POC-HA composites and these values were comparable to those of PLL samples derived from implants in clinical use today. Fibrous capsule thickness of POC-HA samples was minimal and similar to PLL. Unlike POC-HA or POC samples, PLL samples displayed leukocytes at the implant-tissue interface. This study confirms the long-term biocompatibility and favorable tissue ingrowth of POC-HA nanocomposites relative to PLL, and supports their use as bone substitutes or devices for osteochondral regeneration.

Acknowledgments This study was funded by NIH Grant # 1R21EB007355-01 and the National Science Foundation Career Award given to Dr. Guillermo Ameer. The authors wish to thank Dr. Hongjin Qiu, Dr. Daniel Schwartz, Dr. Scott Yang, and Dr. Duk Hwan Ko for their respective contribution to the project.

References

1. Mistry AS, Pham QP, Schouten C, Yeh T, Christenson EM, Mikos AG, Jansen JA. In vivo bone biocompatibility and degradation of porous fumarate-based polymer/alumoxane nanocomposites for bone tissue engineering. J Biomed Mater Res A. 2010;92:451–62.
2. Navarro M, Michiardi A, Castano O, Planell JA. Biomaterials in orthopaedics. J R Soc Interface. 2008;5:1137–58.
3. Wei G, Ma PX. Structure and properties of nano-hydroxyapatite/polymer composite scaffolds for bone tissue engineering. Biomaterials. 2004;25:4749–57.
4. Zhang R, Ma PX. Porous poly(L-lactic acid)/apatite composites created by biomimetic process. J Biomed Mater Res. 1999;45:285–93.
5. Zhang R, Ma PX. Poly(α-hydroxyl acids)/hydroxyapatite porous composites for bone-tissue engineering. I. preparation and morphology. J Biomed Mater Res. 1999;44:446–55.
6. LeGeros RZ. Properties of osteoconductive biomaterials: calcium phosphates. Clin Orthop Relat Res 2002;(395):81–98.
7. Nejati E, Firouzdor V, Eslaminejad MB, Bagheri F. Needle-like nano hydroxyapatite/poly(l-lactide acid) composite scaffold for bone tissue engineering application. Mater Sci Eng C. 2009;29:942–9.
8. Furukawa T, Matsusue Y, Yasunaga T, Shikinami Y, Okuno M, Nakamura T. Biodegradation behavior of ultra-high-strength hydroxyapatite/poly (l-lactide) composite rods for internal fixation of bone fractures. Biomaterials. 2000;21:889–98.
9. Chung EJ, et al. Early tissue response to citric acid-based micro- and nanocomposites. J Biomed Mater Res A;96:29–37.
10. Olszta MJ, et al. Bone structure and formation: a new perspective. Mater Sci Eng. 2007;58:77–116.
11. Fratzl P, Gupta HS, Paschalis EP, Roschger P. Structure and mechanical quality of the collagen-mineral nano-composite in bone. J Mater Chem. 2004;14:2115–23.

12. Rho JY, Kuhn-Spearing L, Zioupos P. Mechanical properties and the hierarchical structure of bone. Med Eng Phys. 1998;20: 92–102.
13. Hutmacher DW, Schantz JT, Lam CXF, Tan KC, Lim TC. State of the art and future directions of scaffold-based bone engineering from a biomaterials perspective. J Tissue Eng Regen Med. 2007; 1:245–60.
14. Qiu H, Yang J, Kodali P, Koh J, Ameer GA. A citric acid-based hydroxyapatite composite for orthopedic implants. Biomaterials. 2006;27:5845–54.
15. Móczó J, Pukánszky B. Polymer micro and nanocomposites: structure, interactions, properties. J Ind Eng Chem. 2008;14: 535–63.
16. Fu S-Y, Feng X-Q, Lauke B, Mai Y-W. Effects of particle size, particle/matrix interface adhesion and particle loading on mechanical properties of particulate-polymer composites. Composites Part B. 2008;39:933–61.
17. Jayabalan M, Shalumon KT, Mitha MK, Ganesan K, Epple M. Effect of hydroxyapatite on the biodegradation and biomechanical stability of polyester nanocomposites for orthopaedic applications. Acta Biomater. 2010;6:763–75.
18. Hasegawa S, et al. A 5–7 year in vivo study of high-strength hydroxyapatite/poly(l-lactide) composite rods for the internal fixation of bone fractures. Biomaterials. 2006;27:1327–32.
19. Ye F, et al. A long-term evaluation of osteoinductive HA/beta-TCP ceramics in vivo: 4.5 years study in pigs. J Mater Sci Mater Med. 2007;18:2173–8.
20. Simion M, Jovanovic SA, Tinti C, Benfenati SP. Long-term evaluation of osseointegrated implants inserted at the time or after vertical ridge augmentation: A retrospective study on 123 implants with 1–5 year follow-up. Clin Oral Implants Res. 2001;12:35–45.
21. Yang J, Webb AR, Ameer GA. Novel citric acid-based biodegradable elastomers for tissue engineering. Adv Mat. 2004;16: 511–6.
22. Niederauer GG, et al. Evaluation of multiphase implants for repair of focal osteochondral defects in goats. Biomaterials. 2000;21:2561–74.
23. Roberts S, McCall I, Darby A, Menage J, Evans H, Harrison P, Richardson J. Autologous chondrocyte implantation for cartilage repair: monitoring its success by magnetic resonance imaging and histology. Arthritis Res Ther. 2003;5:R60–73.
24. Moran M, Kim H, Salter R. Biological resurfacing of full-thickness defects in patellar articular cartilage of the rabbit. Investigation of autogenous periosteal grafts subjected to continuous passive motion. J Bone Joint Surg Br. 1992;74-B:659–67.
25. Goulet RW, Goldstein SA, Ciarelli MJ, Kuhn JL, Brown MB, Feldkamp LA. The relationship between the structural and orthogonal compressive properties of trabecular bone. J Biomech. 1994;27(375–377):379–89.
26. Carter D, Hayes W. The compressive behavior of bone as a two-phase porous structure. J Bone Joint Surg Am. 1977;59:954–62.
27. Swann M. Malignant soft-tissue tumour at the site of a total hip replacement. J Bone Joint Surg Br. 1984;66-B:629–31.
28. Bergsma JE, de Bruijn WC, Rozema FR, Bos RRM, Boering G. Late degradation tissue response to poly(-lactide) bone plates and screws. Biomaterials. 1995;16:25–31.
29. Bergsma EJ, Rozema FR, Bos RRM, Bruijn WCD. Foreign body reactions to resorbable poly(l-lactide) bone plates and screws used for the fixation of unstable zygomatic fractures. J Oral Maxillofac Surg. 1993;51:666–70.
30. Mohamed-Hashem IK, Mitchell DA. Resorbable implants (plates and screws) in orthognathic surgery. J Orthod. 2000;27:198–9.
31. Bostman O, Hirvensalo E, Makinen J, Rokkanen P. Foreign-body reactions to fracture fixation implants of biodegradable synthetic polymers. J Bone Joint Surg Br. 1990;72:592–6.
32. Heidemann W, et al. Degradation of poly(,)lactide implants with or without addition of calciumphosphates in vivo. Biomaterials. 2001;22:2371–81.
33. Bostman OM, Pihlajamaki HK. Adverse tissue reactions to bioabsorbable fixation devices. Clin Orthop Relat Res. 2000;371: 216–27.
34. Bostman OM, Pihlajamaki HK, Partio EK, Rokkanen PU. Clinical biocompatibility and degradation of polylevolactide screws in the ankle. Clin Orthop Relat Res. 1995;320:101–9.
35. Bucholz R, Henry S, Henley M. Fixation with bioabsorbable screws for the treatment of fractures of the ankle. J Bone Joint Surg Am. 1994;76:319–24.
36. Bos RRM, et al. Degradation of and tissue reaction to biodegradable poly(L-lactide) for use as internal fixation of fractures: a study in rats. Biomaterials. 1991;12:32–6.
37. Habraken WJEM, Wolke JGC, Mikos AG, Jansen JA. Injectable PLGA microsphere/calcium phosphate cements: physical properties and degradation characteristics. J Biomater Sci, Polymer Edn. 2006;17:1057–74.
38. Shastri VP, Zelikin A, Hildgen P. Synthesis of synthetic polymers: poly(anhydrides). California: Academic Press; 2002.
39. Rezwan K, Chen QZ, Blaker JJ, Boccaccini AR. Biodegradable and bioactive porous polymer/inorganic composite scaffolds for bone tissue engineering. Biomaterials. 2006;27:3413–31.
40. Unger RE, et al. Tissue-like self-assembly in cocultures of endothelial cells and osteoblasts and the formation of microcapillary-like structures on three-dimensional porous biomaterials. Biomaterials. 2007;28:3965–76.
41. Scherberich A, Galli R, Jaquiery C, Farhadi J, Martin I. Three-dimensional perfusion culture of human adipose tissue-derived endothelial and osteoblastic progenitors generates osteogenic constructs with intrinsic vascularization capacity. Stem Cells. 2007;25:1823–9.
42. Murphy WL, Simmons CA, Kaigler D, Mooney DJ. Bone regeneration via a mineral substrate and induced angiogenesis. J Dent Res. 2004;83:204–10.
43. Pezzatini S, Solito R, Morbidelli L, Lamponi S, Boanini E, Bigi A, Ziche M. The effect of hydroxyapatite nanocrystals on microvascular endothelial cell viability and functions. J Biomed Mater Res A. 2006;76A:656–63.
44. Karin AH, Lester FW, Thomas B. Comparative performance of three ceramic bone graft substitutes. Spine J. 2007;7:475–90.
45. Hunziker EB. Biologic repair of articular cartilage: defect models in experimental animals and matrix requirements. Clin Orthop Relat Res. 1999;367:S135–46.
46. Webb AR, Kumar VA, Ameer GA. Biodegradable poly(diol citrate) nanocomposite elastomers for soft tissue engineering. J Mater Chem. 2007;17:900–6.